

Loss of the chloride channel CIC-7 leads to lysosomal storage disease and neurodegeneration

Dagmar Kasper^{1,5,6}, Rosa Planells-Cases^{1,6,7}, Jens C Fuhrmann^{1,6}, Olaf Scheel¹, Oliver Zeitz², Klaus Ruether^{2,3}, Anja Schmitt¹, Mallorie Poët¹, Robert Steinfeld⁴, Michaela Schweizer¹, Uwe Kornak^{1,8} and Thomas J Jentsch^{1,*}

¹Zentrum für Molekulare Neurobiologie, ZMNH, Universität Hamburg, Hamburg, Germany, ²Augenlinik, Universitätsklinikum Eppendorf, Hamburg, Germany, ³Charité-Virchow-Augenlinik, Berlin, Germany and ⁴Department of Pediatrics, University of Goettingen, Goettingen, Germany

CIC-7 is a chloride channel of late endosomes and lysosomes. In osteoclasts, it may cooperate with H⁺-ATPases in acidifying the resorption lacuna. In mice and man, loss of CIC-7 or the H⁺-ATPase $\alpha 3$ subunit causes osteopetrosis, a disease characterized by defective bone resorption. We show that CIC-7 knockout mice additionally display neurodegeneration and severe lysosomal storage disease despite unchanged lysosomal pH in cultured neurons. Rescuing their bone phenotype by transgenic expression of CIC-7 in osteoclasts moderately increased their lifespan and revealed a further progression of the central nervous system pathology. Histological analysis demonstrated an accumulation of electron-dense material in neurons, autofluorescent structures, microglial activation and astrogliosis. Like in human neuronal ceroid lipofuscinosis, there was a strong accumulation of subunit c of the mitochondrial ATP synthase and increased amounts of lysosomal enzymes. Such alterations were minor or absent in CIC-3 knockout mice, despite a massive neurodegeneration. Osteopetrotic *oc/oc* mice, lacking a functional H⁺-ATPase $\alpha 3$ subunit, showed no comparable retinal or neuronal degeneration. There are important medical implications as defects in the H⁺-ATPase and CIC-7 can underlie human osteopetrosis.

The EMBO Journal (2005) 24, 1079–1091. doi:10.1038/sj.emboj.7600576; Published online 10 February 2005
Subject Categories: neuroscience; molecular biology of disease

Keywords: channelopathy; NCL/*TCIRG1*; transgenic rescue

*Corresponding author. Zentrum für Molekulare Neurobiologie, ZMNH, Universität Hamburg, Falkenried 94, 20246 Hamburg, Germany. Tel.: +49 40 42803 4741; Fax: +49 40 42803 4839; E-mail: Jentsch@zmnh.uni-hamburg.de

⁵Present address: Nordic Bioscience A/S, Herlev 207, 2730 Herlev, Denmark

⁶These authors contributed equally to this work

⁷Present address: Centro Superior en Alta Tecnología Científica, Amadeo de Saboya 4, 46010 Valencia, Spain

⁸Present address: Max-Planck-Institut für Molekulare Genetik, Ihnestr. 63–73, 14195 Berlin, Germany

Received: 13 September 2004; accepted: 14 January 2005; published online: 10 February 2005

Introduction

Several chloride channels of the CLC family play important roles in regulating electrical excitability and transepithelial transport. Over the past few years, however, it emerged that many CLC proteins are expressed in membranes of the endocytotic pathway (Jentsch *et al*, 2002). A common denominator of their function may be the electrical neutralization of protons that are actively pumped into the lumen of intracellular vesicles. The importance of luminal acidification is illustrated by the severe consequences entailed by the mutational inactivation of vesicular CLC channels in mice and men. The disruption of the endosomal CIC-5 channel led to defective renal endocytosis (Piwon *et al*, 2000), resulting in the complex phenotype of a kidney stone disorder (Lloyd *et al*, 1996). Disrupting CIC-3, a channel expressed in endosomes and synaptic vesicles, resulted in a severe degeneration of the hippocampus and in blindness (Stobrawa *et al*, 2001). In both cases, the acidification of specific vesicle populations was significantly reduced (Piwon *et al*, 2000; Stobrawa *et al*, 2001; Yoshikawa *et al*, 2002; Günther *et al*, 2003; Hara-Chikuma *et al*, 2005).

Immunocytochemistry and cell fractionation revealed that the ubiquitously expressed CIC-7 channel (Brandt and Jentsch, 1995) resides in late endosomes and lysosomes (Kornak *et al*, 2001). Mice with a disruption of the corresponding gene *Clcn7* showed severe osteopetrosis, retinal degeneration, and died within 7 weeks (Kornak *et al*, 2001). Their osteopetrosis resulted from defective osteoclasts that failed to acidify the resorption lacuna and hence could not degrade bone. In WT osteoclasts, CIC-7 is inserted together with the V-type H⁺-ATPase into the ruffled border, a specialized, acid-secreting plasma membrane domain. The impaired osteoclast function in *Clcn7*^{-/-} mice may result from a failure to electrically balance proton transport by passive Cl⁻ currents (Kornak *et al*, 2001).

The osteopetrosis of *Clcn7*^{-/-} mice led to the identification of *CLCN7* mutations also in humans. Homozygous mutations lead to malignant infantile osteopetrosis (Kornak *et al*, 2001), whereas patients heterozygous for dominant mutations suffer from a less severe form (Cleiren *et al*, 2001; Frattini *et al*, 2003). Homozygous mutations in the $\alpha 3$ subunit of the H⁺-ATPase also cause severe osteopetrosis both in mice (Li *et al*, 1999; Scimeca *et al*, 2000) and men (Frattini *et al*, 2000; Kornak *et al*, 2000). These genetic findings further support the notion that both the proton pump and the CIC-7 channel are crucial for the acidification of the resorption lacuna.

Besides osteopetrosis, mice lacking CIC-7 display severe retinal degeneration (Kornak *et al*, 2001). Visual impairment is frequently observed in patients with severe infantile osteopetrosis (Steward, 2003) and has often been ascribed to a compression of the optic nerve by the osteopetrotic process. There are a few reports on central nervous system (CNS) degeneration of patients suffering from malignant infantile osteopetrosis (Steward (2003) and references therein),

prompting us to investigate whether the loss of CIC-7 might be associated with a more general degeneration in the nervous system.

We now show that CIC-7 disruption leads to a widespread degeneration of the CNS with typical features of neuronal ceroid lipofuscinosis (NCL), a subtype of human lysosomal storage disease. This suggests that the recently observed neurological abnormalities in several patients with *CLCN7* osteopetrosis (Frattoni *et al*, 2003) are caused by an NCL-like phenotype directly linked to the lack of CIC-7. Although the disruption of CIC-3 also caused severe retinal and CNS degeneration that led to an almost total loss of the hippocampus, we show that this is not associated with the typical signs of lysosomal storage disease in our mouse model (Stobrawa *et al*, 2001). We neither observed retinal nor CNS degeneration in osteopetrotic *oc/oc* mice that carry a mutation in the $\alpha 3$ subunit of the V-type H^+ -ATPase (Scimeca *et al*, 2000). These findings suggest that patients with malignant infantile osteopetrosis carrying mutations in the proton pump may be cured by bone marrow transplantation, whereas patients with a total loss of CIC-7 are likely to develop blindness and severe CNS degeneration even if the osteopetrosis is successfully treated by such an intervention.

Results

CIC-7 resides on neuronal lysosomes

Previous work had shown that CIC-7 is broadly expressed in the mouse embryo, with particularly high levels in the central and peripheral nervous system (Kornak *et al*, 2001). We now determined the expression of CIC-7 in the adult brain using mice expressing a lacZ fusion protein from the endogenous *Clcn7* locus (Kornak *et al*, 2001). LacZ staining revealed CIC-7 expression in virtually every region of the CNS, including the hippocampus, cerebellum and cortex (Figure 1A–C). As exemplified by the strong labeling of the pyramidal cell layer in the hippocampus (Figure 1A) and of Purkinje and granule cells in the cerebellum (Figure 1B), neurons were stained prominently. Expression was also detected in other cells, including ependymal cells and most likely glia. Astrocytes were clearly immunostained for CIC-7 in cell culture (data not shown).

Immunostaining of CIC-7 revealed a punctate pattern in neuronal cell bodies that was absent in CIC-7 knockout (KO) tissue (Figure 1D). Immunogold electron microscopy localized CIC-7 to the limiting membrane of large cytoplasmic vesicles that most likely represent lysosomes (Figure 1E). In cultured hippocampal neurons, CIC-7 was distributed in a punctate pattern in cell bodies and proximal neurites. It nearly perfectly co-localized with lamp-1, a marker for late endosomes and lysosomes (Figure 1F). Hence, CIC-7 resides in late endosomal and lysosomal membranes in fibroblasts (Kornak *et al*, 2001) and neurons.

Neurodegeneration in the CNS of *Clcn7*^{-/-} mice

Histological analysis revealed a conspicuous degeneration of the hippocampal CA3 region of CIC-7 KO mice (Figure 2). A reduction in cell density became visible at postnatal day 20 (p20) (Figure 2C) and in most animals CA3 pyramidal cells were almost completely lost by p30–p40 (Figure 2B). The apparent absence of cell loss at p12 (Figure 2D) argued against a developmental defect. The degeneration was paral-

leled by an activation of microglia, as revealed by GSA staining of the hippocampus (Figure 2F and G). Microglia invaded the pyramidal layer of the CA3, but not of the CA1 region. Similarly, there was increased staining for the astrocyte marker GFAP (Figure 2H and I). No neurodegeneration was visible in osteopetrotic *oc/oc* mice (Figure 2E), which neither showed astrocytosis (not shown). In *Clcn7*^{-/-} mice close to their death around p40, neuronal loss also occurred in the cortex and the number of cerebellar Purkinje cells seemed decreased. To obtain older animals and exclude effects of osteopetrosis on the nervous system, we generated transgenic mice expressing CIC-7 under the control of the tartrate-resistant acid phosphatase (TRAP) promoter that is nearly exclusively active in osteoclasts and macrophages (Schwartzberg *et al*, 1997). Introducing this TRAP::CIC-7 transgene into the *Clcn7*^{-/-} background yielded mice with normal bone density (unpublished data). Their lifespan was prolonged only by 3 weeks (to an age of ~2 months). They displayed severe CNS degeneration that progressed beyond the stage seen in the total KO. At 2 months of age, there was a dramatic reduction in the size of the hippocampus, with its CA3 region totally lacking neuronal cell bodies (Figure 2J and K). The thickness of the neocortex was reduced, and, in the cerebellum, roughly 50% of Purkinje cells were lost (Figure 2L and M).

Retinal degeneration does not depend on the osteopetrosis

Human malignant osteopetrosis is often associated with visual impairment (Steward, 2003). The retina of *Clcn7*^{-/-} mice degenerates within the first 2–4 weeks after birth, leading to an almost complete loss of photoreceptors at p28 (Kornak *et al*, 2001). We now compared the retinal morphology of *Clcn7*^{-/-} and *oc/oc* mice at p30. Unlike the severely degenerated *Clcn7*^{-/-} retina (Figure 3C), the retina of *oc/oc* mice appeared normal (Figure 3B).

To study the functional consequences of retinal degeneration, scotopic electroretinograms (ERGs) were measured in *Clcn7*^{+/-} (control), *Clcn7*^{-/-} and *oc/oc* mice at p24–25 (Figure 3E–G). The early electronegative response of the retina to a light pulse (a-wave) reflects the function of the photoreceptors, while the b-wave represents the response of the second retinal neuron (mainly bipolar cells). Both ERG components were significantly reduced in *Clcn7*^{-/-} mice (Figure 3G and H), but not in *oc/oc* mice at the same age (Figure 3F). As osteopetrosis is equally severe in these mice, we conclude that the retinal degeneration of *Clcn7*^{-/-} mice is not due to optic nerve compression. This conclusion is strongly supported by unchanged retinal degeneration in *Clcn7*^{-/-} mice with a transgenic rescue of the osteopetrosis (Figure 3D).

CNS degeneration in *Clcn7*^{-/-} mice displays features of NCL

Electron microscopy identified electron-dense, osmiophilic material in the perikarya of hippocampal and cortical neurons of p40 *Clcn7*^{-/-} mice (Figure 4A). Already at p11, storage material was abundant in *Clcn7*^{-/-} neurons (data not shown) and increased further with age, whereas no deposits were found in the brains of p30 *oc/oc* mice (Figure 4C). Higher magnification (Figure 4B) revealed a mixed ultrastructure consisting of amorphous, granular or, infrequently, lamellar deposits (Figure 4B, inset). These

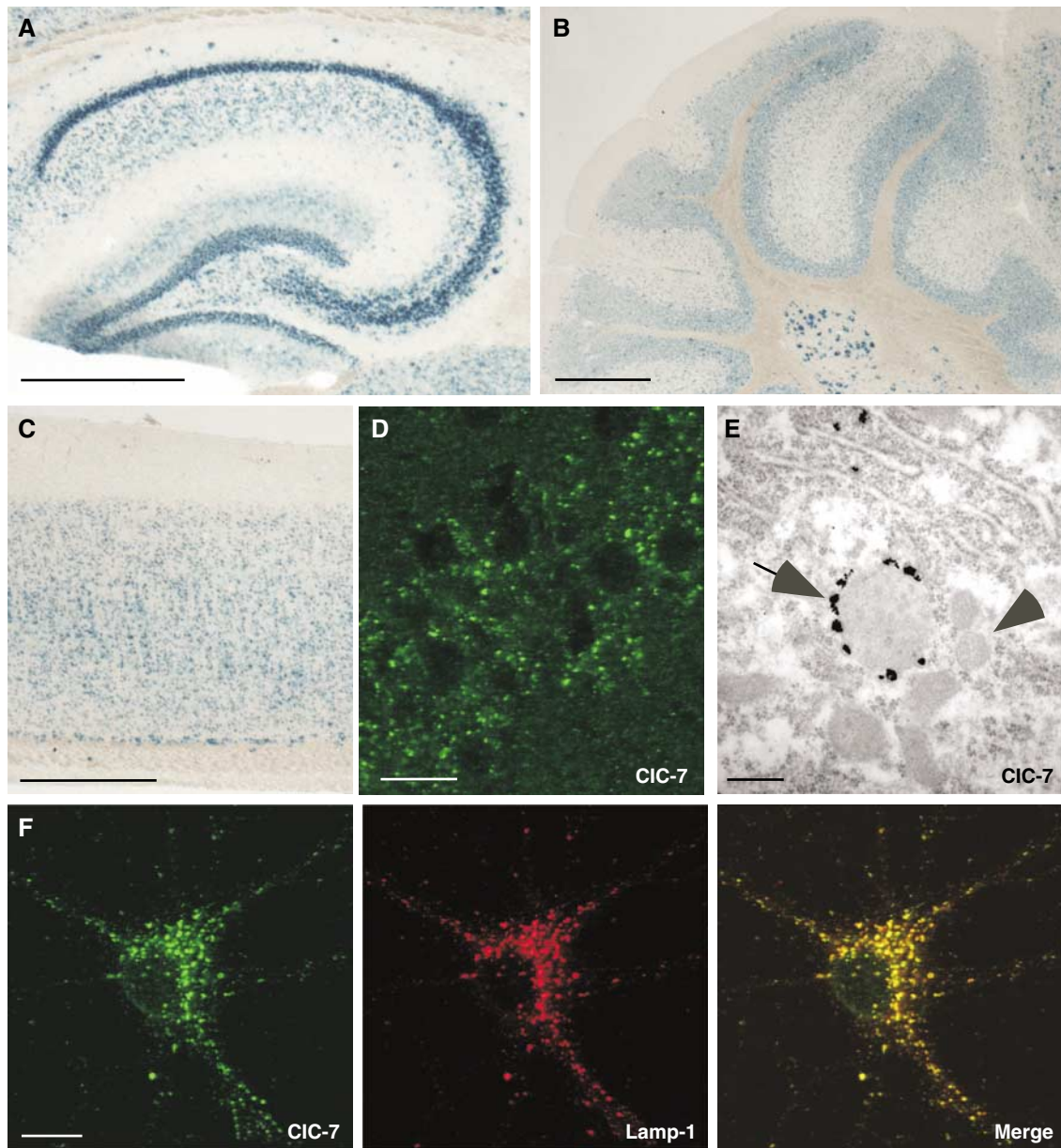


Figure 1 Localization of CIC-7 in the CNS. (A–C) X-gal staining of brain cryosections from mice expressing a CIC-7/lacZ fusion protein. Strong signals were detected in neuronal cell layers of the hippocampus (A), cerebellum (B) and cortex (C). Brains from WT mice were not stained (not shown). Scale bars (A–C): 0.25 mm. (D) Punctate, perinuclear CIC-7 localization in the pyramidal layer of the hippocampal CA1 region as shown by immunofluorescence. Only weak, diffuse staining was present in the CIC-7 KO (not shown). (E) Localization of CIC-7 by immunogold labeling in a cortical neuron. The limiting membrane of a lysosome (arrow) was prominently stained, whereas mitochondria (arrowhead) were devoid of staining. Scale bar: 0.25 μ m. (F) Staining of CIC-7 (green) and lamp-1 (red) in a cultured hippocampal neuron, revealing a large degree of co-localization (yellow). Scale bars for (D, F): 10 μ m.

resembled the avacuolar lipopigments, granular osmiophilic deposits (GROD) and fingerprint profiles observed in variable proportions in a form of human lysosomal storage diseases, the neuronal ceroid lipofuscinoses (NCL) (Goebel and Wisniewski, 2004). Recently, mice disrupted for the homologous Cl^- channel CIC-3 were reported to show storage material and to recapitulate some aspects of NCL (Yoshikawa *et al*, 2002). However, no electron-dense deposits were found in neurons of our *Cln3*^{-/-} mouse model (Stobrawa *et al*, 2001), not even in the regions most severely affected by neurodegeneration (data not shown).

One of the hallmarks of NCL is the presence of autofluorescent pigments (Goebel and Wisniewski, 2004).

Autofluorescence appearing as bright punctae was observed in *Cln7*^{-/-} brains as early as p20 and progressed over time. It was found predominantly in the CA3 region of the hippocampus (Figure 4E, arrow), underneath the corpus callosum, in the cerebral cortex and the thalamus. Its preferential localization in regions of intense GSA staining suggested an association with microglia. Fluorescence of brain sections from *oc/oc* mice (Figure 4F) was not different from WT (Figure 4D), and *Cln3*^{-/-} mice displayed only weak fluorescence in their degenerating hippocampus (Figure 4G). Intracellular carbohydrate accumulation in lysosomal storage diseases can be detected by periodic acid Schiff (PAS) staining (Goebel and Wisniewski, 2004). A perinuclear deposition of carbohydrates was seen in

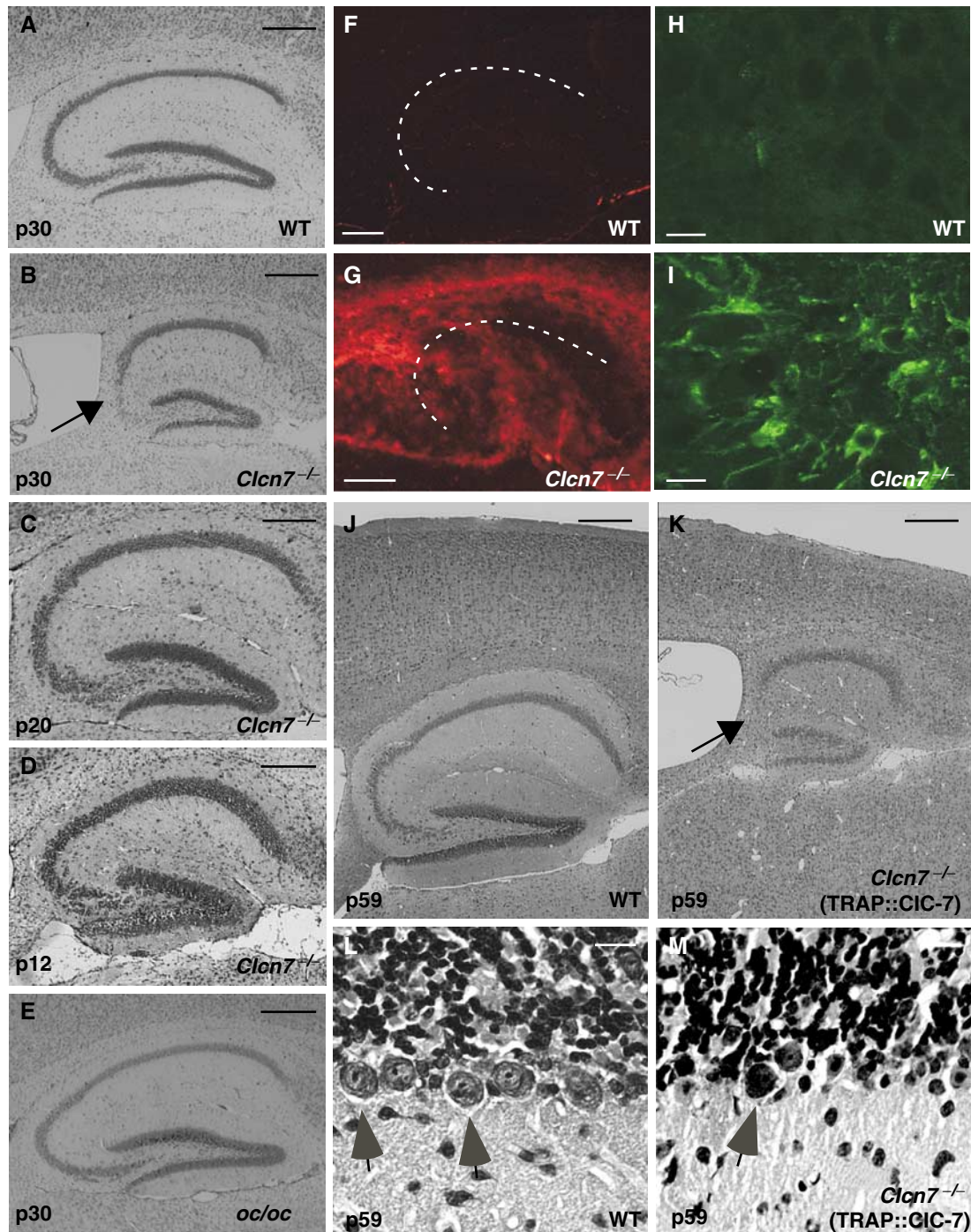


Figure 2 Neurodegeneration in *Clcn7*^{-/-}, but not in *oc/oc* mice. (A–E) Neuronal loss in the hippocampal CA3 region (arrow in B) at p30 as revealed by Nissl staining was found in *Clcn7*^{-/-} mice (B). *oc/oc* mice (E) were similar to WT controls (A). At p12, hippocampal sections of *Clcn7*^{-/-} mice appeared normal (D). A reduction of cell density became visible at p20 (C). These pathological changes were observed in all animals that were analyzed at p30 or older ($n > 8$). Neurodegeneration in *Clcn7*^{-/-} mice was accompanied by increased staining with the microglial marker GSA (F, G; the pyramidal cell layer is indicated by a dashed line) and for the astrocyte marker protein GFAP (H, I). (K) In 2-months-old *Clcn7*^{-/-} mice carrying a TRAP::CLC-7 transgene to rescue osteopetrosis, a further degeneration of cerebral cortex and hippocampus (arrow, CA3 region) is visible in Nissl staining as compared to WT (J). Severe loss of Purkinje cells (arrows) in the cerebellum of *Clcn7*^{-/-} TRAP::CLC-7 mice (M) compared to WT (L) at p59. Scale bars: (A–G, J, K), 0.25 mm; (H, I, L, M), 10 μ m.

cortical neurons of p30 *Clcn7*^{-/-} mice (Figure 4I) and virtually all other brain regions (data not shown). In contrast, PAS staining was increased neither in *oc/oc* (Figure 4J) nor in *Clcn3*^{-/-} (Figure 4K) brain, despite the massive neurodegeneration at that age (3 months) in the latter mice.

As in many forms of human NCL, storage material in *Clcn7*^{-/-} mice was not restricted to neurons. Electron-dense

deposits were prominent in proximal tubule cells of KO, but not WT kidneys (Figure 4L–N). We used immunohistochemistry and postembedding immunogold techniques to further characterize the storage material in *Clcn7*^{-/-} neurons. In *Clcn7*^{-/-} hippocampus and cortex, the lysosomal marker lamp-1 was changed from a WT pattern of discrete cytoplasmic punctae (Figure 5A) to a more diffuse and more

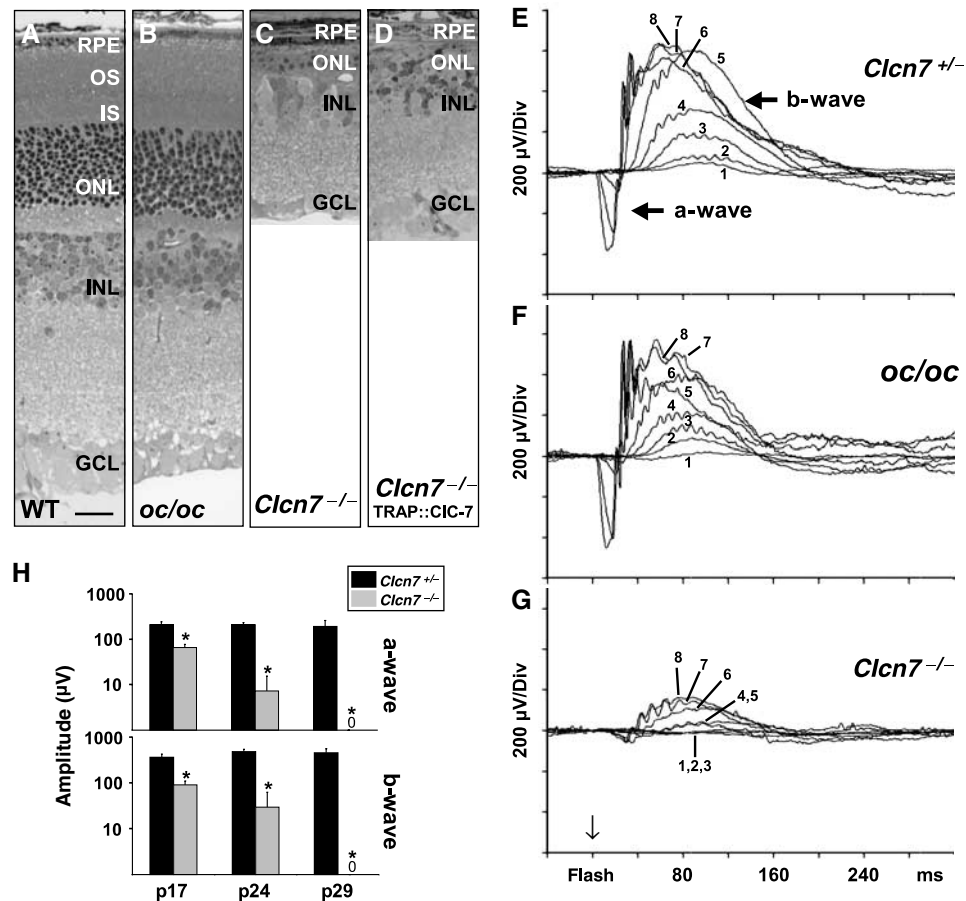


Figure 3 Retinal degeneration in *Clcn7*^{-/-}, but not in *oc/oc* mice. (A–D) Methylene blue-stained semithin retinal sections from WT (A), *oc/oc* (B), *Clcn7*^{-/-} (C) and *Clcn7*^{-/-} TRAP::C1C-7 (D) mice at p30. Scale bar: 20 µm; RPE, retinal pigment epithelium; OS/IS: photoreceptor outer/inner segments; ONL/INL: outer/inner nuclear layer; GCL: ganglion cell layer. (E–G) Scotopic full-field ERGs at p24–25. The electrical responses to different flash energies (indicated by numbers 1–8: 0.1, 0.4, 1, 4, 10, 100, 3000 mcds/m²) are superimposed. There is barely any difference in the response between *Clcn7*^{+/-} (control) (E) and *oc/oc* mice (F). In *Clcn7*^{-/-} mice (G), both a- and b-waves were markedly reduced. (H) Comparison of mean a- and b-wave amplitudes between *Clcn7*^{-/-} and *Clcn7*^{+/-} mice in response to 3000 mcds/m² at p17, p24 and p29. At p29, the electrical response of the retina had virtually disappeared. *n* = 7, 5, 3 for +/- and 6, 5, 4 for KO. Error bars, s.e.m. (**P* < 0.05).

intense staining (Figure 5B). Similar changes were seen for the late endosomal/lysosomal protein saposin D (Figure 5C and D). At the EM level, electron-dense deposits were positive for cathepsin D (Figure 5E), indicating a lysosomal origin. Storage material in most forms of human NCL contains large amounts of subunit c of the mitochondrial ATP synthase. In the WT, immunogold label for subunit c was confined to the mitochondria, whereas in *Clcn7*^{-/-} mice, it was also prominently found on electron-dense storage material (Figure 5F). Western blotting revealed an increase of subunit c in brain lysates from *Clcn7*^{-/-}, but not from *Clcn3*^{-/-} mice (Figure 6H).

Changes in lysosomal enzymes characteristic for NCL

To further characterize the *Clcn7*^{-/-} storage phenotype, we measured several lysosomal enzyme activities. Lysosomal acid phosphatase activity was determined in brain cryosections *in situ* (Figure 6A–D). *Clcn7*^{-/-} mice showed drastically increased staining, which was predominantly localized to neuronal cell bodies (Figure 6B). By contrast, no difference to WT controls (Figure 6A) was found in *oc/oc* (Figure 6D) or in *Clcn3*^{-/-} mice, even when the latter were examined at 3 months of age (Figure 6C). The expression and processing of

the lysosomal protease cathepsin D were assessed by Western blot (Figure 6E). Irrespective of the brain region, intermediate and mature forms of cathepsin D were increased approximately six-fold in *Clcn7*^{-/-} mice. The increase in *Clcn3*^{-/-} mice was ~2-fold, whereas no change of cathepsin D was observed in *oc/oc* mice.

In vitro activities of the lysosomal enzymes β-hexosaminidase and tripeptidyl peptidase I (TPP I) were determined from lysates of different brain regions. Compared to WT, a four- to seven-fold increase in β-hexosaminidase activity was detected in *Clcn7*^{-/-}, but neither in *Clcn3*^{-/-} nor in *oc/oc* mice (Figure 6F). Similarly, *in vitro* TPP I activity was elevated approximately two-fold in *Clcn7*^{-/-} brain but not in *oc/oc*, and only marginally in *Clcn3*^{-/-} mice. β-Hexosaminidase activity was also increased in *Clcn7*^{-/-} liver, heart, kidney, spleen and eye (Figure 6G).

Lysosomal function and pH in living cells

A cell-permeable fluorogenic substrate for TPP I was used to measure lysosomal enzyme activity in living cells. Cleavage of the peptide Ala-Ala-Phe-Rhodamine110-Phe-Ala-Ala resulted in intracellular fluorescence that could be analyzed by FACS. No significant difference was observed between WT

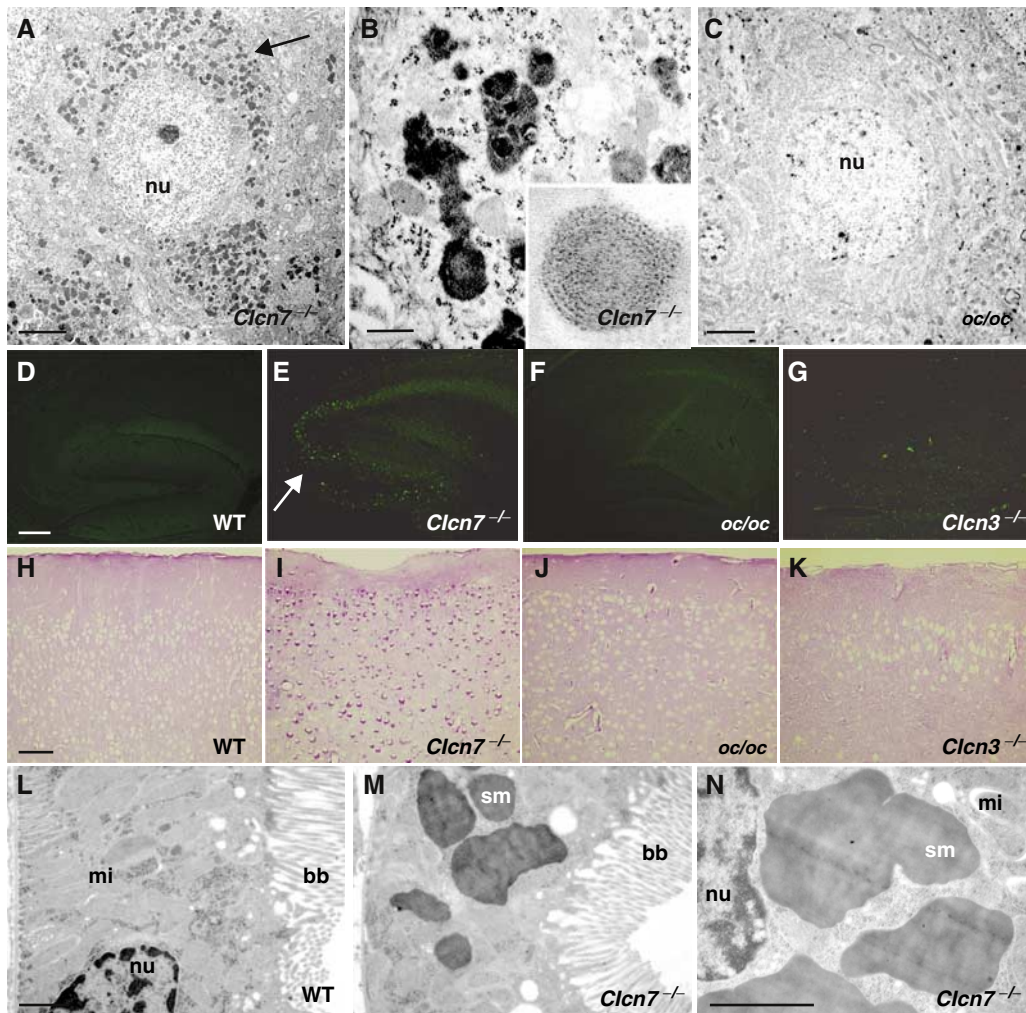


Figure 4 Morphology of lysosomal storage disease in *Clcn7*^{-/-} mice. (A–C) Electron microscopy of cortex sections of p40 *Clcn7*^{-/-} (A, B) and p30 *oc/oc* mice (C). Accumulation of osmiophilic material (arrow) was observed in *Clcn7*^{-/-}, but not in *oc/oc* mice. Higher magnification (B) showed avacuolar lipopigments and, less frequently, lamellar profiles (inset). Scale bars: 2 μ m for (A, C), 200 nm for (B), inset 4 \times . (D–G) Autofluorescence in the hippocampus of *Clcn7*^{-/-} (E, p33, arrow indicates CA3), but not in WT (D, p37) and *oc/oc* (F, p33) mice. Faint autofluorescence was visible in p45 *Clcn3*^{-/-} mice (G). (H–K) PAS staining reveals perinuclear accumulation of carbohydrates in the cortex of p30 *Clcn7*^{-/-} (I), but not in p30 *oc/oc* (J) or in 3-months-old *Clcn3*^{-/-} (K) or WT (H) mice. Scale bars for (D–K): 0.2 mm. (L–N) Electron microscopy of proximal tubular cells from WT (L) and *Clcn7*^{-/-} (M, N) kidneys at p30. Note the electron-dense storage material (sm) in the KO. (bb, brush border; mi, mitochondrion; nu, nucleus). Scale bars: 1.5 μ m.

and *Clcn7*^{-/-} fibroblasts (Figure 7A). TPP I activity of primary neuronal cell cultures was determined by measuring the fluorescent product that was released into the culture medium. There was no difference between WT and KO either (Figure 7B).

Like other vesicular CLC proteins, CLC-7 might provide an electrical shunt for proton pumping (Jentsch *et al*, 2002). We therefore determined lysosomal pH in cultured neurons by ratiometric imaging. The dextrane-coupled pH indicator Oregon green was loaded into cells by endocytosis and chased into late endosomes and lysosomes. Co-staining for lamp-1 confirmed that the dye reached late endosomal/lysosomal compartments in both WT and KO cells (data not shown). The average pH of WT lysosomes was 4.82 ± 0.03 (s.e.m.) and was unchanged in *Clcn7*^{-/-} neurons (pH = 4.82 ± 0.04) (Figure 7C). We neither observed changes in lysosomal pH nor in the delivery of the dye to late endosomes/lysosomes between KO and WT fibroblasts (data not shown).

Changes in gene expression in the hippocampus of *Clcn7*^{-/-} mice

Genome-wide expression profiling was used to detect changes in expression levels in the hippocampi of *Clcn7*^{-/-} mice as compared to WT littermates. It was performed at a time point (p14) before degeneration became obvious. Applying a threshold of 1.5-fold change, 37 transcripts were upregulated and 15 downregulated in the KO. The changes in 25 of the upregulated genes were validated by real-time RT-PCR. In all but one case, this analysis confirmed the qualitative changes observed in the microarray experiments (Table I; for the complete list, see Supplementary data). The genes with increased transcription can be broadly categorized into four classes: genes involved in antigen presentation (MHC class I genes and the proteasome subunit LMP7), complement components, genes with a potential role in microglia/macrophages and often known to be induced by interferons, and finally GFAP, the classical marker of astrocytes. The activation of astrocytes and of components of the

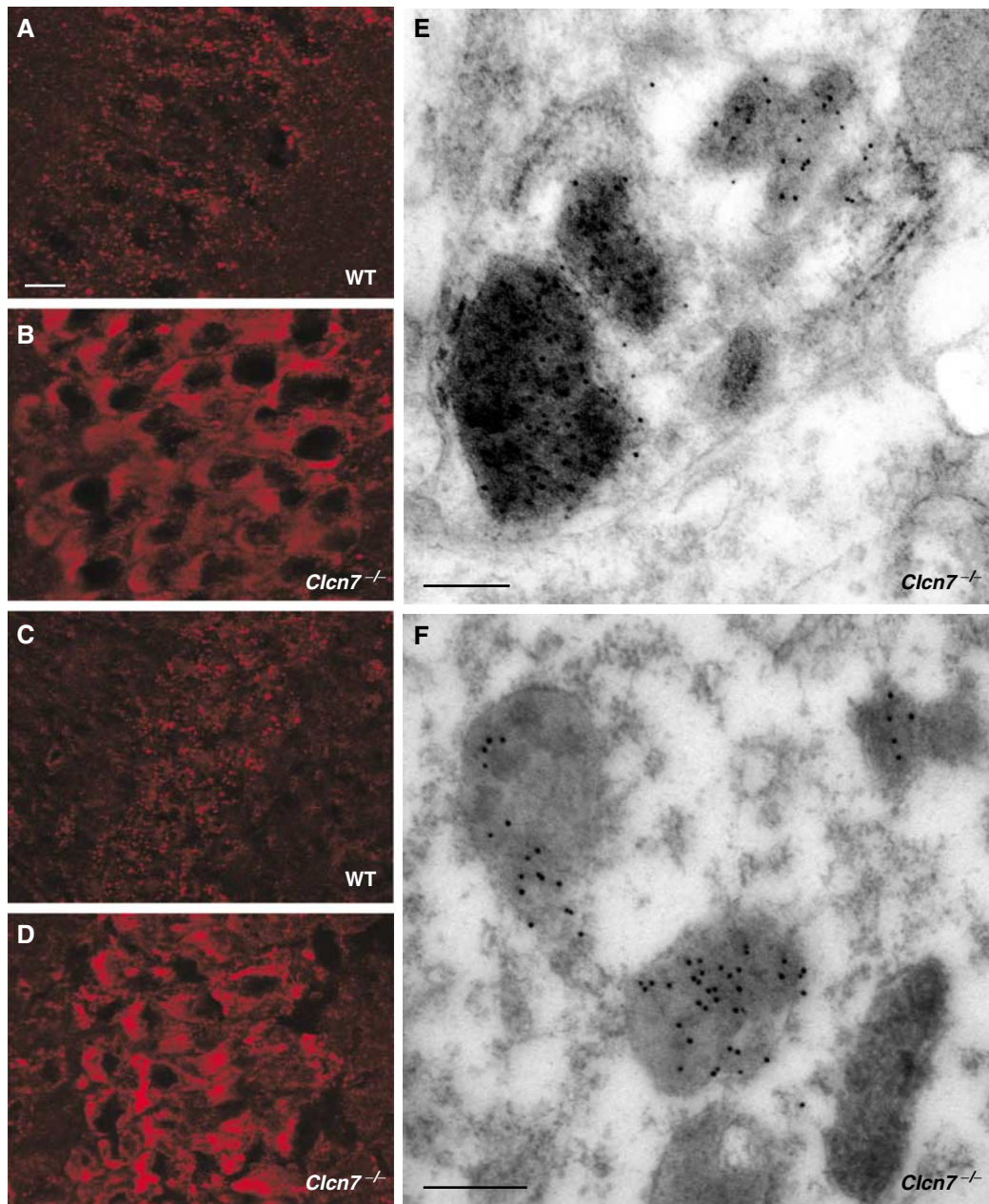


Figure 5 Characterization of lysosomal storage material in *Clcn7*^{-/-} mice. (A–D) Immunostaining for lamp-1 (A, B) and saposin D (C, D) in the CA1 hippocampal region of p30 WT (A, C) and *Clcn7*^{-/-} mice (B, D). Scale bars: 10 μm. (E, F) Postembedding immunogold localization of cathepsin D (E) and subunit c of the mitochondrial ATP synthase (F) in a *Clcn7*^{-/-} neuron. Both proteins are contained within storage deposits characterized by their electron-dense appearance, large size and distorted shape. Scale bars: 0.25 μm.

immune system in *Clcn7*^{-/-} brains, as revealed by expression profiling, are compatible with the microglia activation and astrocytosis described above.

Discussion

Mice lacking CIC-7 show severe osteopetrosis as a consequence of defective HCl secretion by osteoclasts (Kornak *et al*, 2001). Here we describe that the absence of CIC-7 also leads to a severe lysosomal storage phenotype that is associated with neurodegeneration. We compare this phenotype to that of another osteopetrosis model, the osteosclerotic (*oc*) mouse that is deficient in a proton pump subunit, and to that of CIC-

3 KO mice which lack a related endosomal Cl⁻ channel and which also show severe neurodegeneration.

CIC-7 KO has a severe CNS phenotype with signs of NCL

Clcn7^{-/-} mice displayed neurological deficits like hindfeet clapping, which became more severe until the time of death at about 6 weeks. Rescuing the osteopetrotic phenotype by expressing CIC-7 in osteoclasts under the control of the TRAP promoter increased the lifespan of the animals by only a few weeks. Old 'bone rescue' mice showed hypomotility, abnormal postures and a loss of motor control, and lost weight before dying after about 2 months. We assume that severe neurological problems at least contribute strongly to their death.

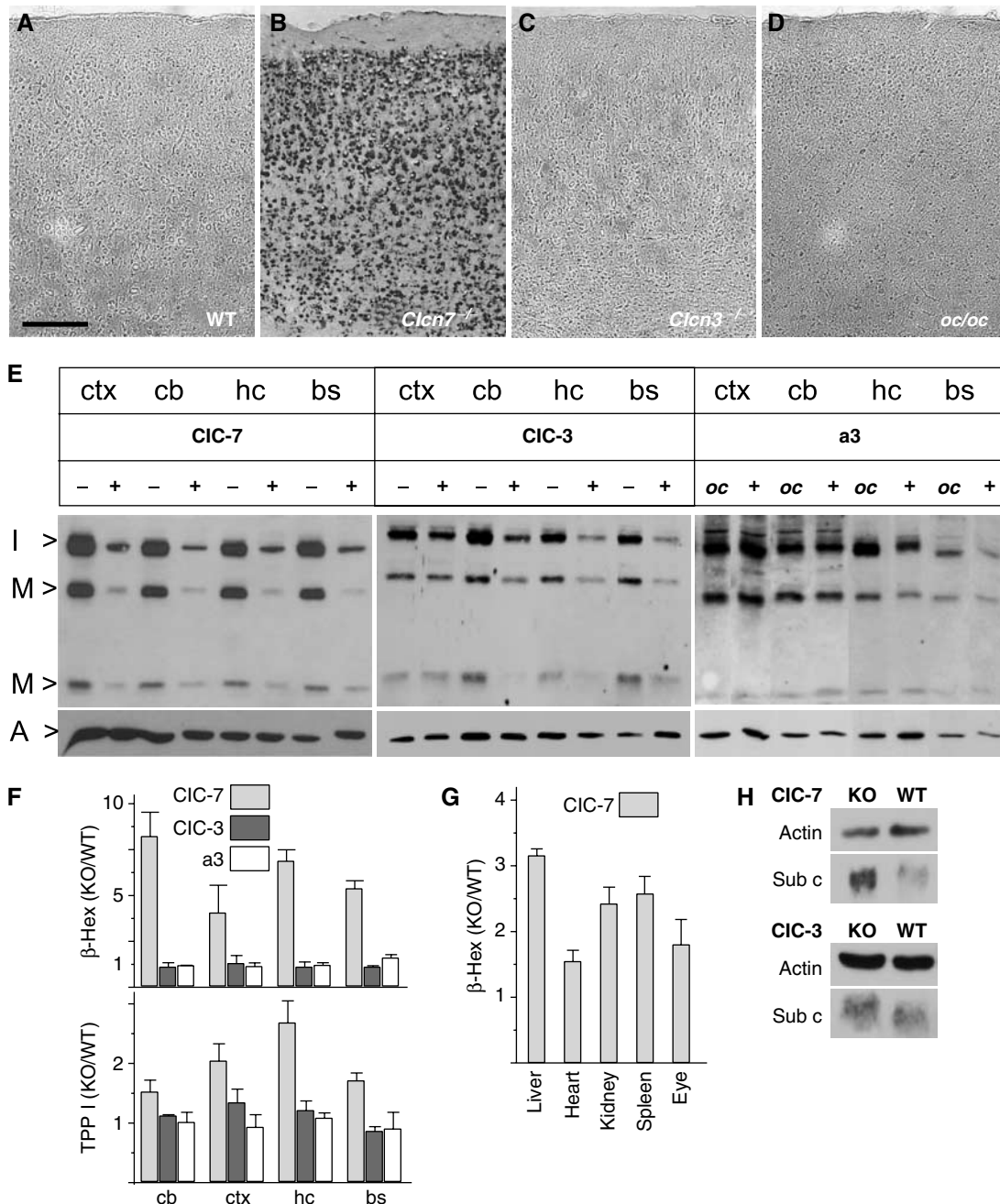


Figure 6 Alteration of lysosomal enzymes in *Clcn7*^{-/-}, but not in *oc/oc* or *Clcn3*^{-/-} mice. (A–D) Lysosomal acid phosphatase activity was visualized *in situ* as dark staining on cortex sections of p40 WT (A), p40 *Clcn7*^{-/-} (B), 3 months *Clcn3*^{-/-} (C) and p29 *oc/oc* mice (D). Scale bar: 20 μm. (E) Immunoblot analysis of cathepsin D. Extracts of different brain regions (ctx, cortex; cb, cerebellum; hc, hippocampus; bs, brainstem) of p30 *Clcn7*^{-/-}, *Clcn3*^{-/-} and *oc/oc* mice were compared to WT controls. Bands represent the intermediate (I>, 42 kDa) and the mature forms (M>, 32 and 12 kDa) of cathepsin D. Staining for actin (A>) served as a loading control. (F) Enzymatic activity of β-hexosaminidase (β-Hex) and TPP I in brain extracts from *Clcn7*^{-/-} (gray bars), *Clcn3*^{-/-} (black bars) and *oc/oc* mice (white bars) at p30 (shown is the ratio of mutant over WT; error bars, s.e.m.; n = 4). (G) Increase of β-hexosaminidase activity in the eye and peripheral organs from *Clcn7*^{-/-} mice. (H) Western blot analysis of subunit c of the mitochondrial ATP synthase of total brain homogenates from *Clcn7*^{-/-}, *Clcn3*^{-/-} and WT mice. Actin served as loading control.

We focused on the cellular basis of the neurological deficits and observed a severe lysosomal storage disease with many typical features of NCL. NCLs are a genetically heterogeneous group of human progressive encephalopathies that are associated with neurocognitive and physical decline and ultimately lead to premature death (Mitchison *et al*, 2004). One of their hallmarks is the neuronal accumulation of autofluorescent lipopigment (Goebel and Wisniewski,

2004). An impairment of lysosomal function has been suggested as a common underlying mechanism. Eight types of NCL are classified according to the age of onset, histological features and genetic loci. The underlying genes, two of which are still unknown, are called CLN1–CLN8. None of these NCL variants is associated with osteopetrosis, making it less likely that *CLCN7* is a candidate for one of the unknown CLN genes.

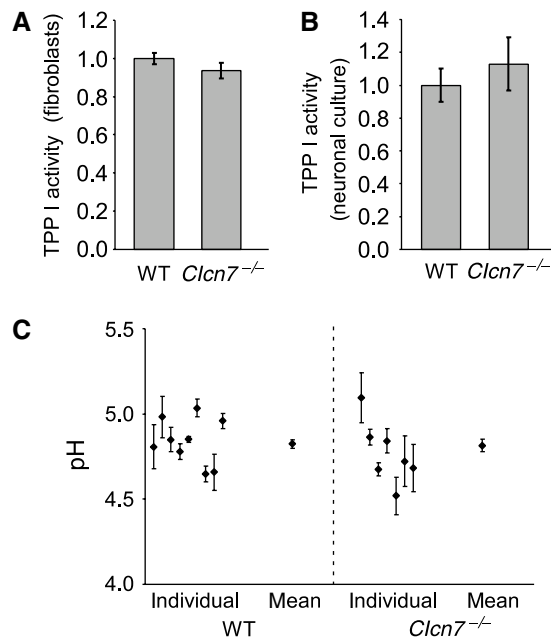


Figure 7 Lysosomal pH and enzyme activity in *Clcn7*^{-/-} cells. (A, B) Measurement of TPP I activity in living cells using Ala-Ala-Phe-Rhodamine110-Phe-Ala-Ala as a substrate. (A) Intracellular fluorescence generated after a 1 h incubation of fibroblasts with the fluorogenic substrate, as analyzed by FACS. (B) TPP I activity in neuronal cultures, as indicated by fluorescence released into the supernatant and normalized to cell density. (C) Lysosomal pH of WT and *Clcn7*^{-/-} neurons was determined with dextran-coupled pH-sensitive dye Oregon green 488 that was loaded by endocytosis. The average pH of WT and KO lysosomes was 4.82 ± 0.03 (s.e.m.) and 4.82 ± 0.04, respectively (*n* = 100 visual fields (containing one to two cells) for WT and 69 for KO; the plot shows pH obtained from individual animals as well as the mean).

Neuronal cell death in the retina and CNS is common to most NCL subtypes. The cortex is affected strongly in all characterized NCL mouse models that frequently display also hippocampal or Purkinje cell loss (Mitchison *et al*, 2004). In *Clcn7*^{-/-} mice, hippocampal (CA3) and cortical neurons as well as Purkinje cells degenerated preferentially, while many other cells, although accumulating storage material, were relatively spared. Cell-intrinsic differences in vulnerability might explain the differential degeneration. Neurodegeneration in *Clcn7*^{-/-} mice was accompanied by microglial activation and astrogliosis, a hallmark of NCL and other CNS pathologies. This was supported by gene expression profiling, which revealed changes similar to those found in mouse models of mucopolysaccharidoses I and IIIB, lysosomal storage diseases associated with neurodegeneration (Ohmi *et al*, 2003). The activation of microglia is probably a consequence of the neuronal pathology and may serve to eliminate dead cells. However, an inappropriate microglial reaction may also have adverse effects as in other degenerative CNS diseases (Wada *et al*, 2000).

Regions affected by neurodegeneration showed increased autofluorescence. In neuronal cell bodies, electron microscopy revealed storage material which displayed heterogeneous morphologies, including amorphous deposits, GRODs and lamellar structures resembling fingerprints. All of these are found in varying proportions in different NCL entities (Goebel and Wisniewski, 2004). In most human

Table 1 Genes upregulated in the *Clcn7*^{-/-} hippocampus

Description	FC
2'-5' Oligoadenylate synthetase-like 2	8.51
Interferon, alpha-inducible protein	6.16
Peptidylprolyl isomerase C-associated protein	3.56
Proteasome subunit, beta type 8 (LMP7)	3.12
Interferon-induced protein with tetratricopeptide repeats 3	2.66
Beta-2 microglobulin	2.63
Guanylate nucleotide-binding protein 3	2.53
Interferon-induced transmembrane protein 3	2.47
Signal transducer and activator of transcription 1	2.45
Sex-limited protein	2.27
Histocompatibility 2, Q region locus 1	2.12
Histocompatibility 2, K region	2.11
Histocompatibility 2, K region	1.95
Interferon regulatory factor 7	1.85
Complement component 1, q subcomponent, beta	1.82
Histocompatibility 2, D region locus 1	1.74
CD52 antigen	1.72
Nuclear factor I/A	1.66
TYRO protein tyrosine kinase-binding protein	1.61
Glial fibrillary acidic protein	1.59
Complement component 1, q subcomponent, gamma	1.57
Interferon-induced protein with tetratricopeptide repeats 1	1.54

Affymetrix chip analysis of genes upregulated in p14 *Clcn7*^{-/-} mouse hippocampus in comparison to WT. Quantification is given as 'fold change' (FC), indicating the increase in KO mice compared to WT. The upregulation of all shown genes was confirmed by real-time RT-PCR. Genes without assigned function and downregulated genes were omitted. The complete list, including RT-PCR data and GeneBank accession, is given in Supplementary data.

NCLs, the major protein accumulating in storage bodies is subunit c of the mitochondrial ATP synthase (Palmer *et al*, 1992; Ezaki and Kominami, 2004). It is believed to be particularly resistant to degradation because of its hydrophobicity. In contrast, saposins are more prominently stored in NCL1 (Tyynelä *et al*, 1993). Levels of both proteins were elevated in *Clcn7*^{-/-} brain and immunogold labeling showed the presence of subunit c in storage material.

Lysosomal function in *Clcn7*^{-/-} mice

Several parameters associated with lysosomal function were altered in *Clcn7*^{-/-} brains. As typically found in NCL (Prasad and Pullarkat, 1996; Sleat *et al*, 1998; Tyynelä *et al*, 2000), the abundance or *in vitro* activity of lysosomal enzymes was increased. Staining for saposin D, which promotes sphingolipid hydrolysis in late endosomes/lysosomes, and for lamp-1, a structural protein of these compartments, suggested an expansion of lysosome-derived structures. Electron microscopy indicated that this apparent expansion was caused by storage material rather than by an increased number of lysosomes.

Despite histological and biochemical findings that are typical for a lysosomal disorder, an analysis of cultured fibroblasts and neurons from *Clcn7*^{-/-} mice failed to reveal defects in lysosome function. No change in lysosomal TPP I activity was observed in living cells. There was no measurable difference in lysosomal pH, neither in cultured neurons nor in fibroblasts. This finding was unexpected, as CIC-7, like other vesicular CLCs, is thought to facilitate vesicular acidification by electrically shunting electrogenic proton pumping (Jentsch *et al*, 2002). A role of CIC-7 in lysosome acidification would also fit to reports that alkalinizing lysosomes by chloroquine caused a neuronal accumulation of lipofuscin-

like storage material (Ivy *et al*, 1984). Although we did not detect differences in lysosomal steady-state pH, we cannot exclude more subtle changes, for example, in the rate of acidification during the travel along the endocytotic-lysosomal pathway. The trafficking along this pathway may depend on its luminal acidification, as evident from the defect in endocytosis in mice lacking the endosomal CIC-5 Cl⁻ channel (Piwon *et al*, 2000). However, we did not detect an obvious defect in targeting the pH indicator to lysosomes, which was an important control for our pH measurements.

However, CIC-7 should be considered a putative Cl⁻ channel, as its absence from the plasma membrane precluded a biophysical characterization. Other potential roles cannot be excluded. For example, CIC-7 might share the transport property of the bacterial homolog CIC-e1, which functions as an electrogenic 2Cl⁻/H⁺ exchanger (Accardi and Miller, 2004). In this case, CIC-7 could still electrically shunt lysosomal proton pumping by mediating Cl⁻ influx, but the lysosomal Cl⁻ accumulation would be directly coupled to the pH gradient. Aside from allowing acidification, little is known about a lysosomal function for chloride. It might drive unknown transport processes across lysosomal membranes or might influence enzymatic activities. For instance, the yeast CLC *gef1p* is thought to raise luminal Cl⁻ in late Golgi compartments, which allosterically influenced the copper loading of an oxidase (Davis-Kaplan *et al*, 1998). Finally, like all mammalian CLCs, CIC-7 has large cytoplasmic domains that may interact with other proteins and that contain CBS domains which may bind ATP (Scott *et al*, 2004). The function of these domains, which carry mutations in several patients with osteopetrosis, is still unknown, but invites speculations.

Consistent with the ubiquitous expression of CIC-7, the lysosomal enzyme β -hexosaminidase was at least moderately increased in every *Clcn7*^{-/-} tissue examined. Similarly, and like in many human forms of NCL (Goebel and Wisniewski, 2004), storage material was not restricted to neurons. Renal proximal tubular cells showed large amounts of deposits, whereas several other cell types expressing comparable levels of CIC-7 were inconspicuous. A possible explanation is that cells characterized by a very high lysosomal activity or a long lifespan are most severely affected. Neurons are nondividing cells that turn over significant amounts of membrane lipid and protein, and proximal tubular cells are highly active in endocytosis and lysosomal degradation of urinary proteins. In view of the high endocytotic load of cells like those of the proximal tubule, a strong impairment of lysosomal degradation would be expected to cause a much more severe pathology than observed in *Clcn7*^{-/-} mice. In this respect, the failure to detect changes in lysosomal function in cell culture, disappointing as it might be, fits well to the disease phenotype. We suggest that the lysosomal dysfunction of *Clcn7*^{-/-} mice is mild, leading to an only slow intracellular accumulation of undigested material in particularly susceptible cells.

Finally, one should address the apparent paradox of impaired lysosomal function (indicated by the accumulation of storage material) in the presence of elevated levels of lysosomal enzymes. This situation is frequently observed in NCL (Ezaki and Kominami, 2004) and is interpreted as an accumulation of enzymes in compartments whose environment is not optimal for their function. Indeed, whereas *in vitro* TPP I activity in extracts from several brain regions was increased,

there was no change of *in vivo* activity measured with a cleavable, fluorogenic substrate.

Retina degeneration separated from the osteopetrosis phenotype

Cell death in the retina of *Clcn7*^{-/-} mice was even more dramatic and occurred faster than in the CNS. In electroretinograms of *Clcn7*^{-/-} mice, the reduction of the a-wave (generated by photoreceptors) was not preceded, but paralleled by a decrease of the b-wave (generated mainly by bipolar cells), consistent with a primary reduction in photoreceptor function. Neither the histological nor the more sensitive electrophysiological analysis indicated a retinal dysfunction in osteopetrotic *oc/oc* mice at p24/25. Together with the equally severe retinal degeneration in transgenic 'bone rescue' animals, this proves that this degeneration is retina-intrinsic in *Clcn7*^{-/-} mice and that the constriction of the optic nerve (Kornak *et al*, 2001) plays a minor role. Instead, the retinal degeneration is probably closely related to the NCL phenotype. Visual impairment and blindness are observed in most subtypes of NCL (Goebel and Wisniewski, 2004). The increased β -hexosaminidase activity in the retina indicates a lysosomal dysfunction also in this tissue, and we detected minor amounts of electron-dense storage material in *Clcn7*^{-/-} ganglion cells (data not shown). Retinal cells might degenerate too fast to allow a more pronounced intracellular storage.

Neurodegeneration in CIC-3 KO mice differs from typical NCL

CIC-3 is a Cl⁻ channel of endosomes and synaptic vesicles (Stobrawa *et al*, 2001) and is important for the acidification of these compartments (Stobrawa *et al*, 2001; Yoshikawa *et al*, 2002). Disruption of CIC-3 led to a severe neurodegeneration in which the hippocampus was nearly totally lost after 3 months (Stobrawa *et al*, 2001; Dickerson *et al*, 2002; Yoshikawa *et al*, 2002). Such an extreme and preferential degeneration of the hippocampus has not been described in human NCL. *Clcn3*^{-/-} mice generated by Yoshikawa *et al* (2002) were reported to display lipofuscin-like granules in the perikarya of hippocampal neurons and increased levels of subunit c in subcellular fractions enriched for lysosomes. In contrast, electron microscopy of hippocampal neurons from our *Clcn3*^{-/-} mice detected signs of cytolysis in the absence of storage material (Stobrawa *et al*, 2001). In these mice, we observed only weak autofluorescence, unchanged total subunit c levels, no change in PAS staining or in lysosomal enzymes, except for a slight increase in cathepsin D. Our electron microscopical analysis of *Clcn3*^{-/-} and *Clcn7*^{-/-} mice was performed in C57Bl/6 and mixed C57Bl/6x129SvJ backgrounds. Only minor differences in the amount of neuronal storage material were seen in the *Clcn7*^{-/-} lines, whereas none of the two different CIC-3 KO lines showed significantly more intracellular electron dense material than was normal for the age (up to 13 months) analyzed. The source of the apparent differences between our *Clcn3*^{-/-} mice (Stobrawa *et al*, 2001) and those of Yoshikawa *et al* (2002) thus remains unclear. The difference in lysosomal pathology between *Clcn7*^{-/-} and *Clcn3*^{-/-} mice, however, correlates with the lysosomal localization of CIC-7 and not CIC-3.

Phenotypic comparison of CIC-7 and a3-deficient mice

Mutations in *CLCN7* (Kornak *et al*, 2001) and *TCIRG1* (*Atp6i*; encoding the a3 subunit of the V-type H⁺-ATPase) (Frattini *et al*, 2000; Kornak *et al*, 2000) are common causes of malignant infantile osteopetrosis in humans, supporting the concept that currents of CIC-7 are required for the acidification of the resorption lacuna (Kornak *et al*, 2001). The gene for the a3 subunit has been disrupted in mice by homologous recombination (Li *et al*, 1999) and bears a deletion in the spontaneous *oc/oc* mouse mutant (Scimeca *et al*, 2000). Both mouse strains develop severe osteopetrosis. Although a3 levels in brain are low, both CIC-7 and a3 are broadly expressed (Nishi and Forgac, 2000; Toyomura *et al*, 2000). In fibroblasts and in macrophage precursors, the a3 subunit has been located in lysosomes (Toyomura *et al*, 2003). Importantly, we show that CNS and primary retinal degeneration are present in *Clcn7*^{-/-} and absent in a3-deficient mice. Thus, a3 can probably be replaced by the homologous a1 or a2 proteins. Both latter subunits are expressed in brain (Nishi and Forgac, 2000; Toyomura *et al*, 2000), although they are believed to be mainly present in endosomes and synaptic vesicles (Morel *et al*, 2003; Toyomura *et al*, 2003).

Absence of CNS and retinal degeneration in *oc/oc* mice: medical implications

The lack of neuronal and retinal degeneration in *oc/oc* mice has potentially important medical implications. As osteopetrosis is equally severe in *oc/oc* and *Clcn7*^{-/-} mice (unpublished results), our comparison of these mouse models and in particular the 'bone rescue' *Clcn7*^{-/-} mice indicate that the blindness and neurodegeneration of *Clcn7*^{-/-} mice are not secondary consequences of their osteopetrosis. Primary retinal and neurodegeneration or lysosomal storage disease were observed in some patients with malignant infantile osteopetrosis (Steward (2003) and references therein). A recent report describes neurological symptoms and brain atrophy in osteopetrotic patients with *CLCN7* mutations (Frattini *et al*, 2003). We conclude that the brain and retina pathology described here is probably present in human malignant osteopetrosis caused by *CLCN7*, but not *TCIRG1* (H⁺-ATPase a3) mutations.

Specific mutations in *CLCN7*, however, cause a less severe recessive intermediate form of osteopetrosis (Campos-Xavier *et al*, 2003) and autosomal dominant osteopetrosis type II (ADOII) (Cleiren *et al*, 2001; Frattini *et al*, 2003). Unlike malignant infantile osteopetrosis, ADOII is not generally associated with visual impairment or blindness, and neurological symptoms and neurodegeneration have not been reported. As CLC channels are dimers, heterozygous dominant-negative mutations can reduce currents to 25% of WT levels (Jentsch *et al*, 2002). The remaining activity may suffice for lysosomal function in neurons, but not for bone resorption by osteoclasts.

Bone marrow transplantation is the only therapy available for recessive malignant infantile osteopetrosis (Gerritsen *et al*, 1994). When performed early enough, it can also prevent the loss of vision that is caused by a compression of the optic nerve. As there were no signs of CNS or retinal degeneration in *oc/oc* mice, a mouse model for a3 H⁺-ATPase deficiency (Scimeca *et al*, 2000), bone marrow transplantation may be an effective cure for this subtype of recessive osteopetrosis. Patients with malignant osteopetrosis due to a total loss of

CIC-7, however, may develop blindness and severe NCL-like neurodegeneration despite transplantation.

Materials and methods

Animals

The generation of *Clcn3*^{-/-} and *Clcn7*^{-/-} mice was described (Kornak *et al*, 2001; Stobrawa *et al*, 2001). Transgenic mice expressing CIC-7 under the control of the TRAP promoter will be described in detail elsewhere. Introducing the TRAP::CIC-7 transgene into the *Clcn7*^{-/-} background normalized their bone density (unpublished data). CIC-7 expression was restricted to osteoclasts and few other tissues (liver and low amounts in kidney) and was undetectable in brain or eye. Analysis was carried out in two independent lines. Osteosclerotic (*oc*) mice (Scimeca *et al*, 2000) were obtained from Jackson Laboratory.

Cell culture

Primary fibroblasts of WT and *Clcn7*^{-/-} mice were from tails of p30 animals. After dissociation with collagenase/dispase, cells were cultured in DMEM containing 10% (w/v) fetal calf serum. Cultures of hippocampal neurons were prepared as described (Fuhrmann *et al*, 2002), but p0 mice were used and plating density was 120 000 cells/14 mm coverslip.

Histology, immunohistochemistry and electron microscopy

Primary antibodies for immunohistochemistry were: rabbit α -cathepsin D (Oncogene), rabbit α -CIC-7 (Kornak *et al*, 2001), rat α -lamp-1 (BD PharMingen), mouse α -GFAP (Roche), goat α -saposin D (gift of K Sandhoff, Bonn) and rabbit α -subunit c (gift of E Kominami, Tokyo). Detailed procedures are described in Supplementary data.

Western blot

Tissues were homogenized in PBS with protease inhibitors (Complete[®], Roche) and cleared by centrifugation at 1000 g. Equal amounts of protein were separated by SDS-PAGE, blotted onto nitrocellulose, and labeled with rabbit α -cathepsin D (gift of R Pohlmann, Münster), rabbit α -subunit c (gift of E Kominami, Tokyo) or rabbit α -actin (Sigma) antibodies. Secondary antibodies were conjugated to HRP (Chemicon) and detected by chemoluminescence (SuperSignalWest, Pierce).

Biochemical assays

TPP I activity in brain homogenates was measured using a fluorometric assay with Ala-Ala-Phe-7-amido-4-methylcoumarin (Sigma) as substrate (Kleijer *et al*, 2001). For β -hexosaminidase activity, the substrate was *p*-nitrophenyl-2-acetamido-2-deoxy- β -D-glucopyranosid (Sigma). Brain homogenate was added to 0.1 M sodium citrate, pH 4.6, containing 0.04% (w/v) Na₂S₂O₈, 0.2% (w/v) BSA, 0.5% (w/v) Triton X-100 and 10 mM substrate. The reaction was stopped with 5 vol of 0.4 M glycine, pH 10.4, and OD₄₀₅ was measured in a spectrophotometer.

TPP I activity in living cells

The activity of TPP I was determined using the cell-permeable substrate Ala-Ala-Phe-Rhodamine110-Phe-Ala-Ala (Bis-AAF-R110, synthesized by ThermoHybaid, Ulm, Germany). Sequential cleavage of the nonfluorescent bisamide substrate by TPP I results in the highly fluorescent rhodamine110. Detailed procedures are available as Supplementary data.

Determination of lysosomal pH

Lysosomal pH was measured using the dextran-coupled pH-sensitive ratiometric dye Oregon Green 448 (Molecular Probes). The procedures for loading the dye into lysosomes by endocytosis and pH measurements by imaging are described in Supplementary data.

Electroretinogram

Mouse electroretinograms (ERGs) were recorded as described (Ruether *et al*, 1997). Briefly, the dark adapted and anesthetized mice got a monopolar contact lens electrode and were placed in a dome. A flash series consisting of eight steps started at 10⁻⁴ cds/m² and reached 3.0 cds/m².

Expression profiling

RNA was extracted from the hippocampi of p14 *Clcn7*^{-/-} mice and control littermates, converted into doubled-stranded cDNA and hybridized to Affymetrix murine genome U74v2 microarrays. A detailed protocol is available as Supplementary data. The microarray data have been submitted to ArrayExpress, accession number E-MEXP-242.

Supplementary data

Supplementary data are available at *The EMBO Journal* Online.

References

Accardi A, Miller C (2004) Secondary active transport mediated by a prokaryotic homologue of CLC Cl⁻ channels. *Nature* **427**: 803–807

Brandt S, Jentsch TJ (1995) CLC-6 and CLC-7 are two novel broadly expressed members of the CLC chloride channel family. *FEBS Lett* **377**: 15–20

Campos-Xavier AB, Saraiva JM, Ribeiro LM, Munnich A, Cormier-Daire V (2003) Chloride channel 7 (*CLCN7*) gene mutations in intermediate autosomal recessive osteopetrosis. *Hum Genet* **112**: 186–189

Cleiren E, Benichou O, Van Hul E, Gram J, Bollerslev J, Singer FR, Beaverson K, Aledo A, Whyte MP, Yoneyama T, deVernejoul MC, Van Hul W (2001) Albers-Schönberg disease (autosomal dominant osteopetrosis, type II) results from mutations in the *CLCN7* chloride channel gene. *Hum Mol Genet* **10**: 2861–2867

Davis-Kaplan SR, Askwith CC, Bengtzen AC, Radisky D, Kaplan J (1998) Chloride is an allosteric effector of copper assembly for the yeast multicopper oxidase Fet3p: an unexpected role for intracellular chloride channels. *Proc Natl Acad Sci USA* **95**: 13641–13645

Dickerson LW, Bonthius DJ, Schutte BC, Yang B, Barna TJ, Bailey MC, Nehrke K, Williamson RA, Lamb FS (2002) Altered GABAergic function accompanies hippocampal degeneration in mice lacking CLC-3 voltage-gated chloride channels. *Brain Res* **958**: 227–250

Ezaki J, Kominami E (2004) The intracellular location and function of proteins of neuronal ceroid lipofuscinoses. *Brain Pathol* **14**: 77–85

Frattini A, Orchard PJ, Sobacchi C, Giliani S, Abinun M, Mattsson JP, Keeling DJ, Andersson AK, Wallbrandt P, Zecca L, Notarangelo LD, Vezzoni P, Villa A (2000) Defects in TCIRG1 subunit of the vacuolar proton pump are responsible for a subset of human autosomal recessive osteopetrosis. *Nat Genet* **25**: 343–346

Frattini A, Pangrazio A, Susani L, Sobacchi C, Mirolo M, Abinun M, Andolina M, Flanagan A, Horwitz EM, Mihci E, Notarangelo LD, Ramenghi U, Teti A, Van Hove J, Vujic D, Young T, Albertini A, Orchard PJ, Vezzoni P, Villa A (2003) Chloride channel *CLCN7* mutations are responsible for severe recessive, dominant, and intermediate osteopetrosis. *J Bone Miner Res* **18**: 1740–1747

Fuhrmann JC, Kins S, Rostaing P, El Far O, Kirsch J, Sheng M, Triller A, Betz H, Kneussel M (2002) Gephyrin interacts with Dynein light chains 1 and 2, components of motor protein complexes. *J Neurosci* **22**: 5393–5402

Gerritsen EJ, Vossen JM, Fasth A, Friedrich W, Morgan G, Padmos A, Vellodi A, Porras O, O'Meara A, Porta F, Bordigoni P, Cant A, Hermans J, Griscelli C, Fischer A (1994) Bone marrow transplantation for autosomal recessive osteopetrosis. A report from the Working Party on Inborn Errors of the European Bone Marrow Transplantation Group. *J Pediatr* **125**: 896–902

Goebel HH, Wisniewski KE (2004) Current state of clinical and morphological features in human NCL. *Brain Pathol* **14**: 61–69

Günther W, Pivon N, Jentsch TJ (2003) The CLC-5 chloride channel knock-out mouse—an animal model for Dent's disease. *Pflügers Arch* **445**: 456–462

Hara-Chikuma M, Yang B, Sonawane ND, Sasaki S, Uchida S, Verkman AS (2005) CLC-3 chloride channels facilitate endosomal acidification and chloride accumulation. *J Biol Chem* **280**: 1241–1247

Ivy GO, Schottler F, Wenzel J, Baudry M, Lynch G (1984) Inhibitors of lysosomal enzymes: accumulation of lipofuscin-like dense bodies in the brain. *Science* **226**: 985–987

Acknowledgements

We thank S Bauer, J Enderich, N Krönke and B Merz for technical assistance, E Becker for work on the rescue construct, and E Kominami (Tokyo), R Pohlmann (Münster) and K Sandhoff (Bonn) for antibodies. This work was supported by grants from the DFG, and the NGFN program of the BMBF. R Planells-Cases was supported by a Marie-Curie fellowship from the European Union and an EMBO short-term fellowship, and M Poët by a Marie-Curie fellowship.

Jentsch TJ, Stein V, Weinreich F, Zdebik AA (2002) Molecular structure and physiological function of chloride channels. *Physiol Rev* **82**: 503–568

Kleijer WJ, van Diggelen OP, Keulemans JL, Losekoot M, Garritsen VH, Stroink H, Majoor-Krakauer D, Franken PF, Eurlings MC, Taschner PE, Los FJ, Galjaard RJ (2001) First-trimester diagnosis of late-infantile neuronal ceroid lipofuscinosis (LINCL) by tripeptidyl peptidase I assay and CLN2 mutation analysis. *Prenat Diagn* **21**: 99–101

Kornak U, Kasper D, Bösl MR, Kaiser E, Schweizer M, Schulz A, Friedrich W, Delling G, Jentsch TJ (2001) Loss of the CLC-7 chloride channel leads to osteopetrosis in mice and man. *Cell* **104**: 205–215

Kornak U, Schulz A, Friedrich W, Uhlhaas S, Kremens B, Voit T, Hasan C, Bode U, Jentsch TJ, Kubisch C (2000) Mutations in the a3 subunit of the vacuolar H⁺-ATPase cause infantile malignant osteopetrosis. *Hum Mol Genet* **9**: 2059–2063

Li YP, Chen W, Liang Y, Li E, Stashenko P (1999) *Atp6i*-deficient mice exhibit severe osteopetrosis due to loss of osteoclast-mediated extracellular acidification. *Nat Genet* **23**: 447–451

Lloyd SE, Pearce SH, Fisher SE, Steinmeyer K, Schwappach B, Scheinman SJ, Harding B, Bolino A, Devoto M, Goodyer P, Rigden SP, Wrong O, Jentsch TJ, Craig IW, Thakker RV (1996) A common molecular basis for three inherited kidney stone diseases. *Nature* **379**: 445–449

Mitchison HM, Lim MJ, Cooper JD (2004) Selectivity and types of cell death in the neuronal ceroid lipofuscinoses. *Brain Pathol* **14**: 86–96

Morel N, Dedieu JC, Philippe JM (2003) Specific sorting of the a1 isoform of the V-H⁺ ATPase a subunit to nerve terminals where it associates with both synaptic vesicles and the presynaptic plasma membrane. *J Cell Sci* **116**: 4751–4762

Nishi T, Forgac M (2000) Molecular cloning and expression of three isoforms of the 100-kDa a subunit of the mouse vacuolar proton-translocating ATPase. *J Biol Chem* **275**: 6824–6830

Ohmi K, Greenberg DS, Rajavel KS, Ryazantsev S, Li HH, Neufeld EF (2003) Activated microglia in cortex of mouse models of mucopolysaccharidoses I and IIIB. *Proc Natl Acad Sci USA* **100**: 1902–1907

Palmer DN, Fearnley IM, Walker JE, Hall NA, Lake BD, Wolfe LS, Haltia M, Martinus RD, Jolly RD (1992) Mitochondrial ATP synthase subunit c storage in the ceroid-lipofuscinoses (Batten disease). *Am J Med Genet* **42**: 561–567

Pivon N, Günther W, Schwake R, Bösl MR, Jentsch TJ (2000) CLC-5 Cl⁻ channel disruption impairs endocytosis in a mouse model for Dent's disease. *Nature* **408**: 369–373

Prasad VV, Pullarkat RK (1996) Brain lysosomal hydrolases in neuronal ceroid-lipofuscinoses. *Mol Chem Neuropathol* **29**: 169–179

Ruether K, van de Pol D, Jaissle G, Berger W, Tornow RP, Zrenner E (1997) Retinoschisislike alterations in the mouse eye caused by gene targeting of the Norrie disease gene. *Invest Ophthalmol Vis Sci* **38**: 710–718

Schwartzberg PL, Xing L, Hoffmann O, Lowell CA, Garrett L, Boyce BF, Varmus HE (1997) Rescue of osteoclast function by transgenic expression of kinase-deficient Src in *src*^{-/-} mutant mice. *Genes Dev* **11**: 2835–2844

Scimeca JC, Franchi A, Trojani C, Parrinello H, Grosgeorge J, Robert C, Jaillon O, Poirier C, Gaudray P, Carle GF (2000) The gene encoding the mouse homologue of the human osteoclast-specific 116-kDa V-ATPase subunit bears a deletion in osteosclerotic (*oc/oc*) mutants. *Bone* **26**: 207–213

- Scott JW, Hawley SA, Green KA, Anis M, Stewart G, Scullion GA, Norman DG, Hardie DG (2004) CBS domains form energy-sensing modules whose binding of adenosine ligands is disrupted by disease mutations. *J Clin Invest* **113**: 274–284
- Sleat DE, Sohar I, Pullarkat PS, Lobel P, Pullarkat RK (1998) Specific alterations in levels of mannose 6-phosphorylated glycoproteins in different neuronal ceroid lipofuscinoses. *Biochem J* **334**: 547–551
- Steward CG (2003) Neurological aspects of osteopetrosis. *Neuropathol Appl Neurobiol* **29**: 87–97
- Stobrawa SM, Breiderhoff T, Takamori S, Engel D, Schweizer M, Zdebik AA, Bösl MR, Ruether K, Jahn H, Draguhn A, Jahn R, Jentsch TJ (2001) Disruption of CLC-3, a chloride channel expressed on synaptic vesicles, leads to a loss of the hippocampus. *Neuron* **29**: 185–196
- Toyomura T, Murata Y, Yamamoto A, Oka T, Sun-Wada GH, Wada Y, Futai M (2003) From lysosomes to the plasma membrane: localization of vacuolar-type H⁺-ATPase with the $\alpha 3$ isoform during osteoclast differentiation. *J Biol Chem* **278**: 22023–22030
- Toyomura T, Oka T, Yamaguchi C, Wada Y, Futai M (2000) Three subunit α isoforms of mouse vacuolar H⁺-ATPase. Preferential expression of the $\alpha 3$ isoform during osteoclast differentiation. *J Biol Chem* **275**: 8760–8765
- Tyynelä J, Palmer DN, Baumann M, Haltia M (1993) Storage of saposins A and D in infantile neuronal ceroid-lipofuscinosis. *FEBS Lett* **330**: 8–12
- Tyynelä J, Sohar I, Sleat DE, Gin RM, Donnelly RJ, Baumann M, Haltia M, Lobel P (2000) A mutation in the ovine cathepsin D gene causes a congenital lysosomal storage disease with profound neurodegeneration. *EMBO J* **19**: 2786–2792
- Wada R, Tiffit CJ, Proia RL (2000) Microglial activation precedes acute neurodegeneration in Sandhoff disease and is suppressed by bone marrow transplantation. *Proc Natl Acad Sci USA* **97**: 10954–10959
- Yoshikawa M, Uchida S, Ezaki J, Rai T, Hayama A, Kobayashi K, Kida Y, Noda M, Koike M, Uchiyama Y, Marumo F, Kominami E, Sasaki S (2002) CLC-3 deficiency leads to phenotypes similar to human neuronal ceroid lipofuscinosis. *Genes Cells* **7**: 597–605